Applied Physics Letters

Selectively boron doped homoepitaxial diamond growth for power device applications

Cite as: Appl. Phys. Lett. **118**, 023504 (2021); https://doi.org/10.1063/5.0031478
Submitted: 01 October 2020 . Accepted: 03 January 2021 . Published Online: 15 January 2021

F. Lloret, D. Eon, E. Bustarret, F. Donatini, and D. Araujo

Applied Physics Letters ARTICLE scitation.org/journal/apl

Selectively boron doped homoepitaxial diamond growth for power device applications

Cite as: Appl. Phys. Lett. **118**, 023504 (2021); doi: 10.1063/5.0031478
Submitted: 1 October 2020 · Accepted: 3 January 2021 ·
Published Online: 15 January 2021

F. Lloret,[1,a] D. Eon,[2] E. Bustarret,[2] F. Donatini,[2] and D. Araujo[3]

AFFILIATIONS

[1]Department of Applied Physics, University of Cádiz, 11510 Puerto Real, Cádiz, Spain
[2]University Grenoble-Alpes, Institut Neél, 38000 Grenoble, France
[3]Department of Material Science, University of Cádiz, 11510 Puerto Real, Cádiz, Spain

Note: This paper is part of the Special Topic on Ultrawide Bandgap Semiconductors.
[a]**Author to whom correspondence should be addressed:** fernando.lloret@uca.es

ABSTRACT

Diamond lateral growth is a powerful technique for the design and fabrication of diamond-based power electronic devices. Growth orientation affects the diamond deposition in terms of growth rate, surface roughness, and impurity incorporation. It has been shown that the finally grown surface of a patterned substrate can be predesigned based on the growth conditions. Thus, simultaneous growth along different surface orientations yields regions with different properties. In line with this, the incorporation of boron in a microwave plasma enhanced chemical vapor deposition laterally deposited epilayer over a mesa patterned {100}-oriented diamond substrate was studied by cathodoluminescence. It was observed that laterally oriented facets were highly boron doped in contrast to the {100}-oriented surfaces, which did not show any bound exciton emission, related to the doping. This study shows that, by designing the initial pattern and tuning the conditions, it is possible to drive a selective incorporation of boron into the grown layer.

Diamond has been widely claimed to be the ultimate semiconductor for power device applications. However, the improvement of power electronics depends not only on the intrinsic characteristics of the semiconductor but also on the architecture of the device.[1,2] A decisive improvement of its electrical characteristics is expected from a three-dimensional (3D) design. 3D architectures allow us to reduce the electric field within the material, which enables operation at higher voltages. Moreover, better material qualities (dopant incorporation, generation of defects, etc.) can be achieved by using other growth directions (such as ⟨111⟩ or ⟨311⟩) combined with that of the substrate.[3] 3D devices offer many advantages, such as low-specific on-resistance,[4] a high breakdown voltage (VB), and a smaller size.[4–6]

These features have raised interest in developing devices based on mesa structures.[5–10] Recently, lateral diamond growth has been proposed for this purpose.[11,12] These works showed that, by tuning the growing conditions, it was possible to grow along a specific orientation on patterned substrates. This method is not only valid for the design of new architectures but also for the control and reduction of dislocations.[13,14]

In this contribution, the effect of lateral growth on the incorporation of impurities is evaluated. A thin boron-doped layer grown laterally over a mesa patterned substrate was investigated by cathodoluminescence (CL). Boron doping modifies the electronic properties of diamond, pinning the Fermi level and incorporating acceptor levels in the bandgap, progressing as the doping increases to an impurity band merging with the valence band above the metallic transition. The CL setup collects the photon generated by the interaction of the incident electrons with the electrons in the sample. The consecutive radiative recombination spectrum depends on the electronic properties of the sample. In particular, at low temperature, excitons bound to boron impurities have specific spectral signatures that make it possible to determine the boron doping levels over a wide range.[15–19] In fact, there is a competition between free exciton and bound exciton recombination channels in the doped regions. When the CL spectrum is recorded in a doped layer, the shorter radiative lifetime of the bound excitons results in a dominant peak centered on their recombination energy, ≈5.22 eV. In diamond, due to the indirect character of the gap, the exciton recombinations involve transverse optical (TO) or transverse acoustic (TA) or longitudinal optical phonons. These phonons allow us to match momentum and imply a weak probability of radiative recombination that results in longer radiative lifetimes. In addition,

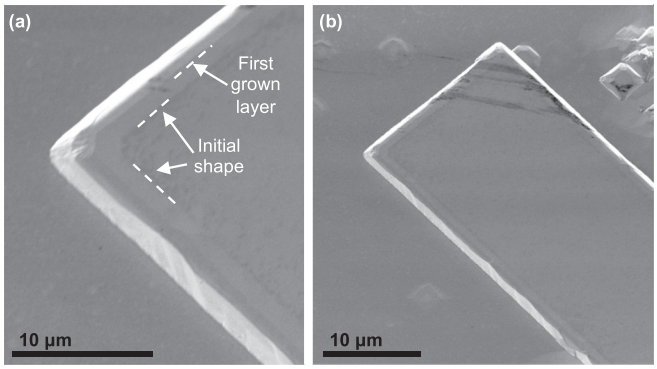

FIG. 1. SEM micrographs of the grown sample tilted 35°. Two contrasts are observed, one attributed to the initial shape and another, less obvious, due to the change in the surface orientation. Both are visible at the edges of the structure and marked in (a).

weak bound exciton luminescence without phonon (NP) assistance is also usually observed, less intense and at a higher energy than that involving phonons.[19] In some cases, the transitions also exhibit zone centered optical phonon replicas (TO+O). The latter are commonly observed in highly boron-doped samples.[17] Consequently, doped regions can be easily identified by CL using the emission of the bound excitons.

For this purpose, one {100}-oriented High-Power High-Pressure (HPHT) diamond substrate from Sumitomo Electric has been etched 1 μm by inductively coupled plasma reactive ion etching (ICP-RIE) with rectangular patterns (30 μm × 1 mm). Pure oxygen gas was used for the plasma etching, with a coil power of 1000 W, a substrate holder power of 40 W, and a gas flow of 100 sccm, at a pressure of 10 mTorr. After chemical cleaning, the patterned substrate was homoepitaxially grown by microwave plasma-enhanced chemical vapor deposition (MW PE CVD). A first undoped layer was deposited for 3 h using a methane concentration of $CH_4/H_2 = 0.1\%$ at a total flux of 200 sccm. A thin doped layer was then grown on top for 8 min. It was grown at $CH_4/H_2 = 0.25\%$ and using diborane as a boron source with a concentration of [B]/[C] = 2.8%. The MW power of 260 W used during the growth of both layers resulted in a temperature of 900 °C as measured using an ISR 6-TI advanced infrared pyrometer from Lumasense Technologies. The working pressure was set at 33 Torr for the whole process. These conditions were chosen to favor lateral growth, i.e., growth along a different orientation from that of the substrate {100}.[12] The sample surface was studied by scanning electron microscopy (SEM) using a FESEM Zeiss Ultra plus microscope at an accelerating voltage of 5 kV. CL spectra were recorded at 4 K using a helium cryostat in an FEI Quanta 200 SEM equipped with a parabolic mirror for collecting and focusing of the light and a Jobin Yvon HR460 grating (600 g/mm) monochromator associated with either a photomultiplier or a CCD (256 × 1024 matrix pixels) camera.

MW PE CVD diamond deposition under the conditions described above resulted in a lateral growth with clear faceting along the {011} orientations.[20] Figure 1 shows an SEM micrograph of the surface of the sample where part of a mesa rectangle appears after the growth process. The sample was tilted 35° to better see the lateral growth at the edges of the mesa. In the micrographs, a lighter contrast was also evidenced. This contrast is attributed to the initial shape of the rectangle prior to any deposition. It is likely due to different local electrical characteristics related to the boron contents in the regions. Figure 1(a) shows one of the corners with higher detail. A second contrast, less obvious, was also observed. It is probably due to the changes in the growth orientation during the first and prolonged step of the deposition process.[11,12]

In order to clarify this point and evaluate the boron-doped layer deposited on the top of the sample, CL spectra at different positions of the sample were recorded. Figure 2(a) shows an SEM micrograph of the sample with the positions where the spectra were recorded marked by colored crosses and labels A, B, C, and D. These positions correspond to outside (A) or within (D) the mesa rectangle, to the lateral side of the mesa (B), and to the upper corner (C). The spectra are shown in Fig. 2(b), where the region of energies corresponding to the bound exciton (BE^{TO}) and the free exciton (FE^{TO}) is enlarged in the inset. These spectra illustrate the different electrical behaviors present in the sample. A and D positions show spectra of nondoped diamond

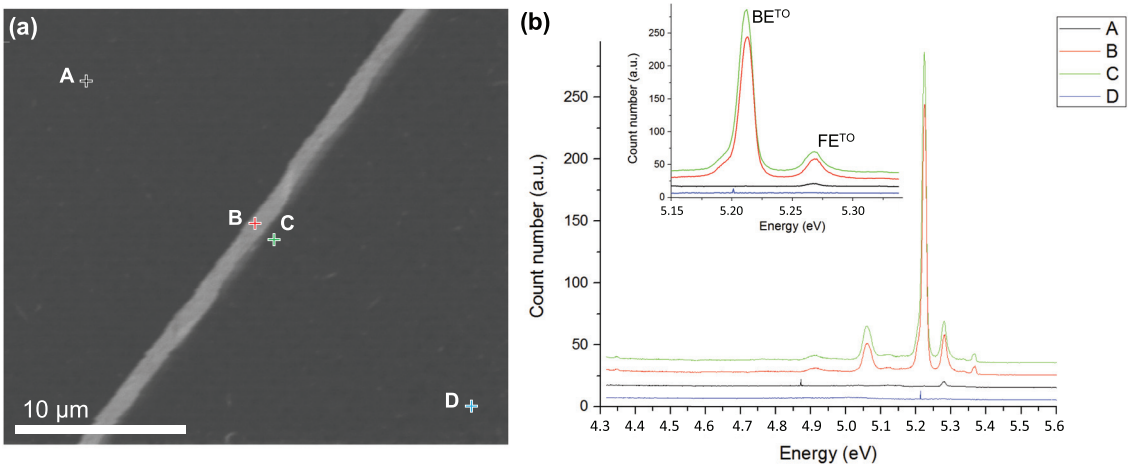

FIG. 2. (a) SEM micrograph of the region where spectra are recorded with the specific positions marked. (b) CL spectra of the four positions shown in the SEM micrograph.

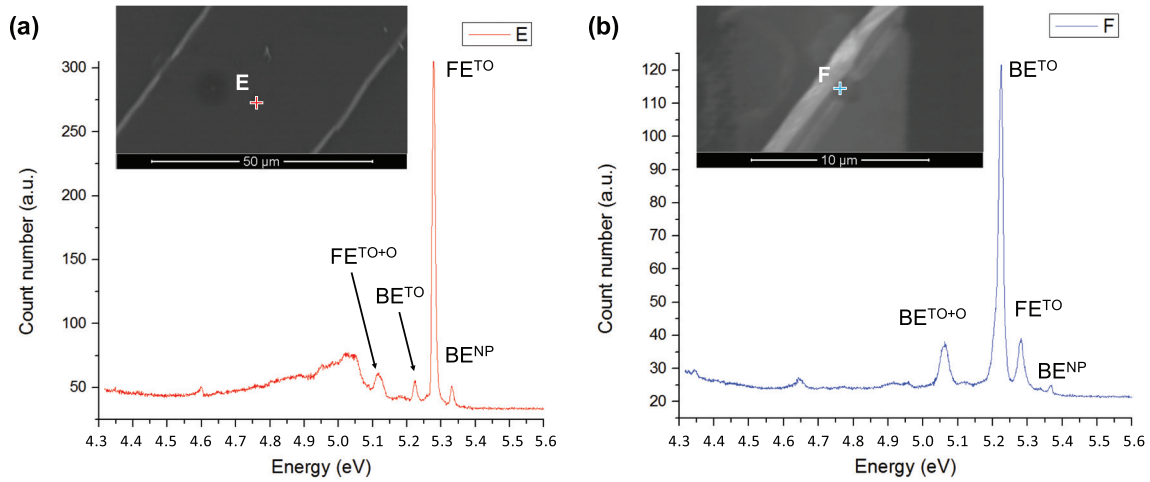

FIG. 3. CL spectrum at the positions marked with a cross in the SEM micrographs is shown in the inset. (a) Spectrum recorded in an area of the sample growth vertically along the (100) orientation. (b) Spectrum recorded in an area of the sample growth laterally. Main peaks are identified.

with a few weak emitter peaks, typical from bad-quality substrates. In contrast, B and C show clearly the BE^{NP}, FE^{TO}, and FE^{TO+O} peaks at the energies of 5.354 eV, 5.265 eV, and 5.106 eV, respectively. BE^{TO} and BE^{TO+O} peaks were detected at 5.207 eV and 5.042 eV, respectively, for B, and 5.208 eV and 5.043 eV, respectively, for C. An $FE^{TO+2^{\circ}}$ signal was also observed in both spectra at around 4.898 eV.

These spectra show a large bound exciton peak, characteristic of doping, only in some regions of the sample (B and C positions). However, the absence of any exciton signal in the other regions may be related to a bad crystalline quality. A high density of defects would result in a nonradiative recombination of the carriers. In order to check if the spectra obtained in A and D are due to the bad quality of the substrate at these positions, additional CL spectra have been recorded. Figure 3 shows spectra obtained at two other positions, (a) E and (b) F, marked in the SEM micrographs in the inset. Position E, Fig. 3(a), yields a very intense FE^{TO} emission at 5.265 eV. BE^{NP}, BE^{TO}, and FE^{TO+O} are also identified with lower emission at the energies of 5.317 eV, 5.210 eV, and 5.101 eV, respectively. In contrast, position F, Fig. 3(b), yields a spectrum where the BE^{TO} peak is the dominant exciton, with an energy of 5.208 eV. BE^{NP} (5.352 eV), FE^{TO} (5.265 eV), and BE^{TO+O} (5.046 eV) were also recorded. In both cases, excitons are observed. However, the bound exciton emission is clearly predominant at position F, while the free exciton is the main peak at E. This shows a similar crystal quality in both regions but points to a clearly different doping level. Such doping levels can be estimated using the ratio of the BE^{TO} and FE^{TO} peak intensities.[21] From this analysis, boron incorporated in the E region (position analogous to D in Fig. 2) resulted in 3×10^{15} cm^{-3}. This value is the minimum boron concentration expected in nonintentionally doped layers grown without boron precursors but using a reactor contaminated with residual boron atoms. Thus, for our setup, this corresponds to usual values obtained for undoped diamond, i.e., nonintentionally doped diamond. On the other hand, carrying out the same analysis on region F resulted in a boron content estimated at 2×10^{17} cm^{-3}. Both values are also in good agreement with the relationship reported by other authors between the BE^{TO} energy position and the boron incorporation.[16]

To further study this growth behavior and show this up over an extended region, monochromatic CL mapping at the BE^{TO} energy has been carried out. Figure 4 shows a region of the sample with a corner of one of the mesa rectangles by SEM in (a) secondary electron (SE) mode and (b) by monochromatic CL micrograph at 5.210 eV. The white signal in the SE image corresponds to the lateral planes of the mesa. The places where the bound exciton was detected are shown in Fig. 4(b) with a white contrast. Monochromatic CL maps looked similar to the SEM micrographs. It is because bound exciton emissions were coming from the edges of the mesa rectangle.

Therefore, the monochromatic mapping at the BE^{TO} peak energy over this sample showed a selective doping, i.e., a fully selective growth of a highly boron doped layer place exclusively present on the lateral facets. It is known that samples grown with low methane concentrations have a quite low growth rate.[20] Extrapolating growth rates for undoped diamond obtained in previous works,[20] layer thicknesses of 96 nm and 8 nm are expected on the {111} lateral planes and the 100 surface orientation (i.e., at positions F and E in Fig. 3), respectively. Considering that the layer grown was doped with boron, these thicknesses are expected to be much less[22] and, therefore, negligible on the {100} planes.

In order to determine if a 8-nm-thick boron-doped diamond layer can be detected by CL, a Monte Carlo simulation has been

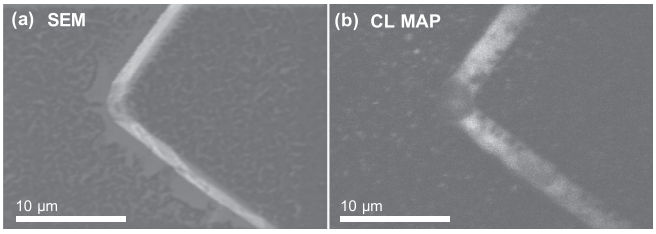

FIG. 4. (a) SE-SEM micrograph of one of the corners of a mesa rectangle. (b) Monochromatic CL map of the BE^{TO} peak (5.210 eV) corresponding to the same region of the sample.

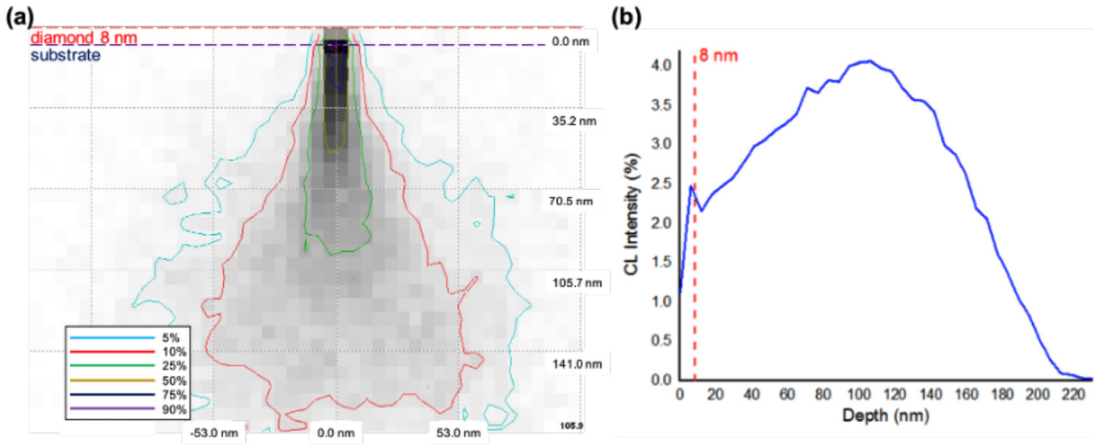

FIG. 5. (a) Monte Carlo simulation of the energy by position in a 5 keV accelerating voltage beam impinging a bilayered diamond sample. (b) CL intensity per depth of the same simulation.

carried out using Casino software. A bilayer composed of two diamond layers, one of 8 nm thickness and another labeled substrate, has been chosen to reproduce the sample. A microscope beam acceleration voltage of 5 keV, the same value as experimentally used, was selected in order to simulate a total number of 2000 trajectories. Figure 5(a) shows the energy by position inside the sample, while the emitted CL intensity was plotted against the penetration depth in the sample in Fig. 5(b). The red dashed line indicates the 8 nm layer depth in both figures. The characteristic pear-shaped interaction volume is well observed in Fig. 5(a). This figure illustrates the respective contribution of the substrate and of the layer to the resulting CL spectrum. Indeed, integrating over the areas in Fig. 5(b), 5% of the total CL signal is coming from the first 8 nm depth. Assuming a deposition of 8-nm-thick 2×10^{17} cm^{-3} boron-doped diamond, the hypothetical resulting CL spectrum should correspond to that of a 10^{16} cm^{-3} doping level (i.e., 20 time less, 5%) recorded on a thick (>250 nm) diamond layer. This is clearly not the case as the experimentally obtained spectrum corresponds to a boron doping level of 3×10^{15} cm^{-3}. Thus, using an e-beam accelerating voltage of 5 kV, CL is sufficiently sensitive to detect an 8-nm-thick 2×10^{17} cm^{-3} doped layer if it were present. Taking this into account and considering that the doping level deduced from the CL spectrum of region E corresponds to that of the residual boron doping of the reactor, we can state that, in the present case, not any boron-doped layer was deposited on the {100}-oriented surface. In the same way, doping values obtained for position F were likely underestimated because the doped layer was probably thinner than 200 nm and the spectral contribution from the intrinsic layer placed below.

This work demonstrates that selective doping is possible over the patterned substrate along specific orientations using growth conditions maximizing the dependence of the growth rate on the growth orientation. A longer growth would eventually result in planarized 100-oriented layers with buried 3D locally doped regions. Subsequent etching processes that can be undertaken in the same CVD reactor using an O_2 plasma would provide access to these regions while maintaining the planar surface. Therefore, this result paves the way for power electronic device designs where photolithography steps should be avoided.

This work was co-financed by the 2014–2020 ERDF Operational Programme and by the Department of Economy, Knowledge, and Business and University of the Regional Government of Andalusia, Project reference: FEDER-UCA18-107851. The authors also would like to thank the Ministerio de Economia y Competitividad (MINECO) of the Spanish Government for funding under Grant Nos. TEC2017-86347-C2-1-R and ESP2017-91820-EXP.

DATA AVAILABILITY

The data that support the findings of this study are available from the corresponding author upon reasonable request.

REFERENCES

[1]N. Donato, N. Rouger, J. Pernot, G. Longobardi, and F. Udrea, J. Phys. D **53**(9), 093001 (2020).
[2]A. Aleksov, M. Kubovic, N. Kaeb, U. Spitzberg, A. Bergmaier, G. Dollinger, Th. Bauer, M. Schreck, B. Stritzker, and E. Kohn, Diamond Relat. Mater. **12**, 391–398 (2003).
[3]A. Tallaire, O. Brinza, V. Mille, L. William, and J. Achard, Adv. Mater. **29**, 1604823 (2017).
[4]H. Umezawa, M. Nagase, Y. Kato, and S. Shikata, Diamond Relat. Mater. **24**, 201 (2012).
[5]Y. Hoshino, H. Kato, T. Makino, M. Ogura, T. Iwasaki, M. Hatano, and S. Yamasaki, Phys. Status Solidi A **209**(9), 1761 (2012).
[6]K. Sato, T. Iwasaki, Y. Hoshino, H. Kato, T. Makino, M. Ogura, S. Yamasaki, S. Nakamura, J. Ichikawa, A. Sawabe, and M. Hatano, Jpn. J. Appl. Phys., Part 1 **53**, 05FP01 (2014).
[7]G. Biasol, A. Gustafsson, K. Leifer, and E. Kapon, Phys. Rev. B **65**, 205306 (2002).
[8]H. Kato, T. Makino, M. Ogura, D. Takeuchi, and S. Yamasaki, Diamond Relat. Mater. **27-28**, 19 (2012).
[9]Y. Ando, T. Kamano, K. Suzuki, and A. Sawabe, Jpn. J. Appl. Phys., Part 1 **51**, 090101 (2012).
[10]D. Takeuchi, T. Makino, H. Kato, M. Ogura, N. Tokuda, T. Matsumoto, D. Kuwabara, H. Okushi, and S. Yamasaki, Phys. Status Solidi A **211**, 2251 (2014).
[11]F. Lloret, A. Fiori, D. Araujo, D. Eon, M. P. Villar, and E. Bustarret, Appl. Phys. Lett. **108**, 181901 (2016).
[12]F. Lloret, D. Araujo, D. Eon, and E. Bustarret, Cryst. Growth Des. **18**(12), 7628–7632 (2018).

[13]A. Boussadi, A. Tallaire, M. Kasu, J. Barjon, and J. Achard, Diamond Relat. Mater. **83**, 162 (2018).
[14]F. Lloret, M. Gutierrez, D. Araujo, D. Eon, and E. Bustarret, Phys. Status Solidi A **214**, 1700242 (2017).
[15]C. Baron, M. Wade, A. Deneuville, F. Jomard, and J. Chevallier, Diamond Relat. Mater. **15**, 597 (2006).
[16]S. Ghodbane, F. Omnès, and C. Agnès, Diamond Relat. Mater. **19**, 273 (2010).
[17]A. Deneuville, C. Baron, S. Ghodbane, and C. Agnès, Diamond Relat. Mater. **16**, 915 (2007).
[18]C. Baron, M. Wade, A. Deneuville, E. Bustarret, T. Kocinievski, J. Chevalier, C. Uzan-Saguy, R. Kalish, and J. Butler, Diamond Relat. Mater. **14**, 350 (2005).
[19]J. Barjon, Phys. Status Solidi A **214**, 1700402 (2017).
[20]F. Lloret, D. Araujo, D. Eon, M. P. Villar, J. M. Gonzalez-Leal, and E. Bustarret, Phys. Status Solidi A **213**(10), 2570 (2016).
[21]F. Omnès, P. Muret, P.-N. Volpe, M. Wade, J. Pernot, and F. Jomard, Diamond Relat. Mater. **20**, 912 (2011).
[22]Y. Zou and K. Larsson, J. Phys. Chem. C **120**, 10658 (2016).